

# WASP-31b: a low-density planet transiting a metal-poor, late-F-type dwarf star<sup>★</sup>, <sup>★★</sup>

D. R. Anderson<sup>1</sup>, A. Collier Cameron<sup>2</sup>, C. Hellier<sup>1</sup>, M. Lendl<sup>3</sup>, T. A. Lister<sup>4</sup>, P. F. L. Maxted<sup>1</sup>, D. Queloz<sup>3</sup>, B. Smalley<sup>1</sup>, A. M. S. Smith<sup>1</sup>, A. H. M. J. Triaud<sup>3</sup>, R. G. West<sup>5</sup>, D. J. A. Brown<sup>2</sup>, M. Gillon<sup>6</sup>, F. Pepe<sup>3</sup>, D. Pollacco<sup>7</sup>, D. Ségransan<sup>3</sup>, R. A. Street<sup>4</sup>, and S. Udry<sup>3</sup>

<sup>1</sup> Astrophysics Group, Keele University, Staffordshire ST5 5BG, UK  
e-mail: dra@astro.keele.ac.uk

<sup>2</sup> SUPA, School of Physics and Astronomy, University of St. Andrews, North Haugh, Fife KY16 9SS, UK

<sup>3</sup> Observatoire de Genève, Université de Genève, 51 Chemin des Maillettes, 1290 Sauverny, Switzerland

<sup>4</sup> Las Cumbres Observatory, 6740 Cortona Dr. Suite 102, Santa Barbara, CA 93117, USA

<sup>5</sup> Department of Physics and Astronomy, University of Leicester, Leicester LE1 7RH, UK

<sup>6</sup> Institut d'Astrophysique et de Géophysique, Université de Liège, Allée du 6 Août, 17, Bat. B5C, Liège 1, Belgium

<sup>7</sup> Astrophysics Research Centre, School of Mathematics & Physics, Queen's University, University Road, Belfast BT7 1NN, UK

Received 25 November 2010 / Accepted 18 May 2011

## ABSTRACT

We report the discovery of the low-density, transiting giant planet WASP-31b. The planet is 0.48 Jupiter masses and 1.55 Jupiter radii. It is in a 3.4-day orbit around a metal-poor, late-F-type,  $V = 11.7$  dwarf star, which is a member of a common proper motion pair. In terms of its low density, WASP-31b is second only to WASP-17b, which is a more highly irradiated planet of similar mass.

**Key words.** binaries: eclipsing – planetary systems – stars: individual: WASP-31

## 1. Introduction

To date, 107 transiting extrasolar planets have been discovered<sup>1</sup>, the majority of which are gas giants in short orbits. The radii of a subset of these exoplanets are larger than predicted by standard models of irradiated gas giants (e.g., Burrows et al. 2007; Fortney et al. 2007), including TrES-4b (Mandushev et al. 2007; Sozzetti et al. 2009), WASP-12b (Hebb et al. 2009), and WASP-17b (Anderson et al. 2010, 2011b). A number of mechanisms have been proposed as potential solutions to the radius anomaly (see Fortney et al. (2010) for a review), each of which involves either injecting heat into the planet from an external source or slowing heat loss from the planet.

One such mechanism is the dissipation of energy within a planet as heat during the tidal circularisation of an eccentric orbit (Bodenheimer et al. 2001; Gu et al. 2003; Jackson et al. 2008; Ibgui & Burrows 2009). Such studies suggest that tidal heating may be sufficient to explain the large radii of even the most bloated exoplanets, though we would have to be observing some systems at very special times. A high heating rate, as suggested by Leconte et al. (2010), would mean most tidal energy is radiated away by the age typical of the very most bloated planets (a few Gyr) and so could not have played a significant role in

their observed bloating. However, the current uncertainty in tidal theory allows for a wide range of heating rates (e.g. Ibgui et al. 2011). Though most studies have considered a transient phase of tidal heating, ongoing tidal heating (e.g. Ibgui et al. 2010) would occur if an additional companion continues to excite the orbital eccentricity of the bloated planet (e.g. Mardling 2007).

Burrows et al. (2007) proposed that enhanced opacities would retard the loss of internal heat and thus slow contraction of bloated planets. They suggested that enhanced opacities may arise due to the strong optical and UV irradiation of short-orbit, gas giants that could alter their atmospheres, producing thick hazes, absorbing clouds and non-equilibrium chemical species (e.g. tholins or polyacetylenes).

The bloated planets are all very strongly irradiated by their host stars, and a small fraction of stellar insolation energy would be sufficient to account for the observed degrees of bloating. Guillot & Showman (2002) suggested that the kinetic energy of strong winds, induced in the atmosphere by the large day-night temperature contrasts that result from tidal locking, may be transported downward and deposited as thermal energy in the deep interior. However, a mechanism to convert the kinetic energy into thermal energy would still be required. Li & Goodman (2010) and Youdin & Mitchell (2010) found that turbulence is efficient at dissipating kinetic energy. Magnetic drag on weakly ionized winds (Perna et al. 2010) and Ohmic heating (Batygin & Stevenson 2010) are alternative mechanisms. The non-bloated planets are also highly irradiated. Hence, such a mechanism would either have to act more efficiently on the bloated planets, or some other property must counteract its effect. One such possibility is the presence of a massive core. Indeed, Guillot et al. (2006) and Burrows et al. (2007) found a correlation between the core masses required to reproduce the

<sup>★</sup> Based in part on observations made with the HARPS spectrograph on the 3.6-m ESO telescope (proposal 085.C-0393) and with the CORALIE spectrograph and the Euler camera on the 1.2-m Euler Swiss telescope, both at the ESO La Silla Observatory, Chile.

<sup>★★</sup> The photometric time-series and radial-velocity data used in this work are only available in electronic form at the CDS via anonymous ftp to cdsarc.u-strasbg.fr (130.79.128.5) or via <http://cdsarc.u-strasbg.fr/viz-bin/qcat?J/A+A/531/A60>

<sup>1</sup> 2010 Nov 25, <http://exoplanet.eu>

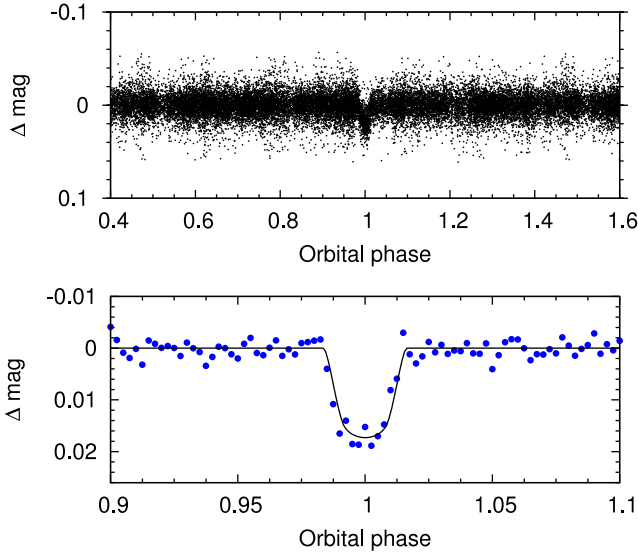


**Fig. 1.** WASP-South discovery light curve. *Upper panel:* Photometry folded on the orbital period of  $P = 3.4$  d. Points with error above three times the median error (0.012 mag) were clipped for display purposes. *Lower panel:* Photometry folded on the orbital period and binned in phase ( $\Delta\phi = 0.025$ ), with the transit model generated from the parameters of Table 4 superimposed.

**Table 1.** Proper motions of WASP-31 and its visual companion

Star	Catalogue	$\mu_{RA}$ (mas)	$\mu_{Dec}$ (mas)
WASP-31	UCAC3	$-28.2 \pm 1.3$	$-0.4 \pm 1.6$
WASP-31	PPXML	$-25.0 \pm 2.3$	$-0.1 \pm 2.4$
Companion	UCAC3	$-33.1 \pm 3.1$	$+1.0 \pm 3.8$
Companion	PPXML	$-28.5 \pm 4.2$	$+1.6 \pm 4.2$

observed radii of known exoplanets and the metallicities of their host stars.

In this paper, we present the discovery of the bloated, transiting, giant planet WASP-31b. Compared to the ensemble of known short-period planets, WASP-31b is moderately irradiated by its low-metallicity host star.

## 2. Observations

WASP-31 is a  $V = 11.7$ , F7–8 dwarf star located in the constellation Crater. WASP-31 has been observed by WASP-South (Pollacco et al. 2006) during the first five months of each year since the start of full-scale operations (2006 May 4). A transit search (Collier Cameron et al. 2006) of the resulting 24 614 usable photometric measurements (Figure 1) found a strong, 3.4-d periodicity.

WASP-31 is a visual double with a  $V \sim 15.8$  star (2MASS 11174477-1903521) approximately  $35''$  away. The 2MASS colours of the companion suggest that it is a mid-to-late K-type star. The proper motions for the two stars listed in the PPMXL (Roeser et al. 2010) and UCAC3 (Zacharias et al. 2010) catalogues suggest that this is a common proper motion pair (Table 1). The companion is blended with WASP-31 in the WASP images, so we corrected the WASP photometry for this contamination to prevent dilution of the transit.

Using the CORALIE spectrograph mounted on the 1.2-m Euler-Swiss telescope (Baranne et al. 1996; Queloz et al. 2000b), we obtained 34 spectra of WASP-31 during 2009 and a

further 13 spectra during 2010. As pressure variations can cause CORALIE to drift on short timescales, we calibrated the stellar spectra by obtaining simultaneous spectra of a thorium-argon lamp. In April 2010, we obtained an additional 10 spectra with the HARPS spectrograph mounted on the 3.6-m ESO telescope. As HARPS is stable at the  $1 \text{ m s}^{-1} \text{ night}^{-1}$  level, we obtained a calibration at the start of each night of observations. This avoids contamination of the stellar spectra by the thorium-argon lamp. The CORALIE measurement taken at  $\text{BJD} = 2\,454\,971.548671$  and the HARPS measurement taken at  $\text{BJD} = 2\,455\,299.716991$  were both affected by cloud cover.

The typical signal-to-noise ratio (S/N) per pixel at 550 nm is 18 for the CORALIE spectra, with exposure times of 30 min, and 26 for the HARPS spectra, with exposure times of 15 min. Radial-velocity (RV) measurements were computed by weighted cross-correlation (Baranne et al. 1996; Pepe et al. 2005) with a numerical G2-spectral template. RV variations were detected with the same period found from the WASP photometry and with a semi-amplitude of  $58 \text{ m s}^{-1}$ , consistent with a planetary-mass companion. The RV measurements are plotted in the upper panel of Figure 2.

To test the hypothesis that the RV variations are due to spectral line distortions caused by the presence of cool stellar spots or a blended eclipsing binary, a line-bisector analysis (Queloz et al. 2001; Santos et al. 2002) of the CORALIE and HARPS cross-correlation functions was performed. The lack of correlation between bisector span and RV (Figure 2, lower panel), especially for the high-precision HARPS measurements, supports the identification of the transiting body as a planet. As an additional test for spots or a blend, we also computed CORALIE RVs by weighted cross-correlation with a numerical K5-spectral template. The amplitude and phase of the RV variations are the same within errors, irrespective of the choice of cross-correlation mask, as would be expected if the variations were caused by the presence of a planet (e.g. Huélamo et al. 2008).

To refine the system parameters, we obtained high-S/N transit photometry. Photometric follow-up observations of WASP-31 were obtained with the LCOGT<sup>2</sup> 2.0-m Faulkes Telescope North (FTN) on Mt. Haleakala, Maui on the night of 2010 Feb 26. The fs03 Spectral Instruments camera was used with a  $2 \times 2$  binning mode, giving a field of view of  $10' \times 10'$  and a pixel scale of  $0.303'' \text{ pixel}^{-1}$ . The data were taken through a Pan-STARRS  $z$  filter, with the telescope defocussed to minimise flat-fielding errors and to allow 60-s exposure times to be used without saturating.

The data were pre-processed using the WASP Pipeline (Pollacco et al. 2006) to perform masterbias and flat construction, debiasing and flatfielding. Due to the very low dark current of the fs03 Fairchild CCD ( $< 0.0001 \text{ e}^- \text{ pix}^{-1} \text{ s}^{-1}$ ), dark subtraction was not performed. Aperture photometry was performed using DAOPHOT within the IRAF environment using an aperture with a radius of 11 pixels. Differential photometry was then performed relative to 20 comparison stars that were within the FTN field of view (Figure 3). The RMS of the residuals about the best-fitting model (Section 4) was 1.4 mmag.

On 2010 April 15 we obtained 4.1 hours of photometry in the Gunn  $r$  filter with the CCD camera on the Euler-Swiss telescope, covering from 40 min before the start of transit until 55 min after it ended. The conditions were variable, with seeing of 0.6–1.7'' and an airmass range of 1.15–1.34. Euler now employs absolute tracking to keep the stars on the same pixels during a whole transit. By identifying point sources in each image and

<sup>2</sup> <http://lcogt.net>

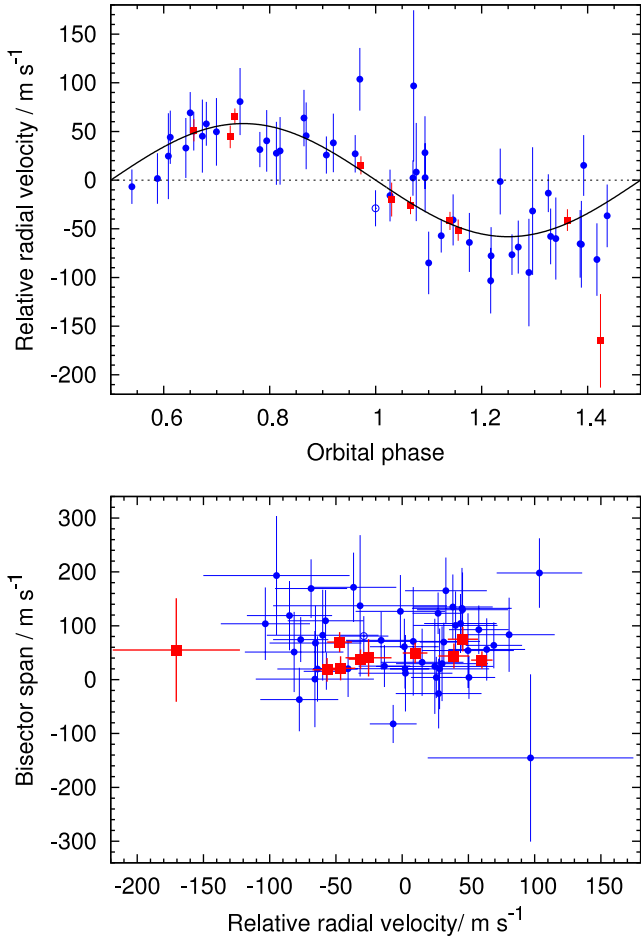


**Fig. 2.** *Upper panel:* Spectroscopic orbit of WASP-31, as illustrated by radial velocities from CORALIE (blue circles) and HARPS (red squares). The best-fitting Keplerian model, generated from the parameters of Table 4, is overplotted as a solid line. An RV taken at BJD = 2 455 168.8468, depicted in the plot by an open circle, fell during transit. As we did not treat the Rossiter-McLaughlin effect (e.g., Queloz et al. 2000a), we excluded this measurement from our combined analysis. *Lower panel:* A lack of correlation between bisector spans and radial velocities rules out a blended eclipsing binary or starspots as the cause of the photometric and spectroscopic variations. We adopted uncertainties on the bisector spans twice the size of those on the radial velocities. For both plots, the centre-of-mass velocity,  $\gamma = -124.92 \text{ m s}^{-1}$ , was subtracted from the radial velocities and the Keplerian model.

matching them with a catalogue, the image centre is calculated. Drifts from the nominal position are then corrected by adjusting the telescope pointing between exposures.

After bias-subtracting and flat-fielding the images, we performed aperture photometry. The flux was extracted for all stars in the field and the final light curve (Figure 3) was obtained by differential photometry of the target and a reference source obtained by combining the 4 brightest reference stars. The RMS of the residuals about the best-fitting model (Section 4) was 2.6 mmag, which was limited by the number of available reference stars.

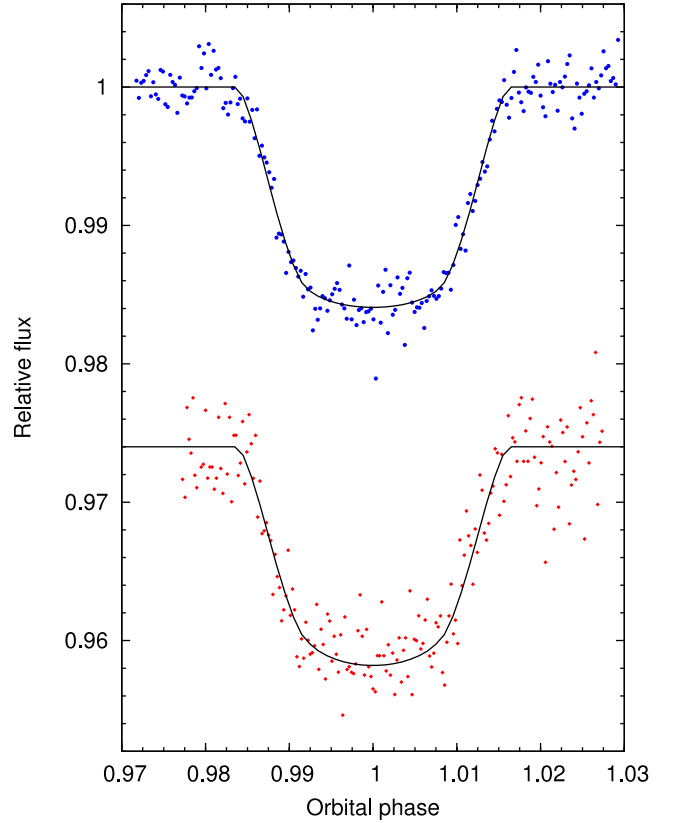


**Fig. 3.** High-S/N transit light curves. The upper observations (blue circles) were obtained by FTN, using a Pan-STARRS  $z$  filter, on 2010 Feb 26. The lower observations (red diamonds), offset in relative flux by 0.026 for display, were obtained by Euler, using a Gunn  $r$  filter, on 2010 Apr 15. The best-fitting transit models generated from the parameters of Table 4 are overplotted.

### 3. Stellar parameters

The individual HARPS spectra of WASP-31 were co-added to produce a single spectrum with an average S/N of around 100:1. The analysis was performed using the methods given in Gillon et al. (2009). The  $H_\alpha$  line was used to determine the effective temperature ( $T_{\text{eff}}$ ), while the Na I D and Mg I b lines were used as surface gravity ( $\log g_*$ ) diagnostics. The parameters obtained from the analysis are listed in Table 2. The elemental abundances were determined from equivalent width measurements of several clean and unblended lines. A value for microturbulence ( $\xi_t$ ) was determined from Fe I using the method of Magain (1984). The quoted error estimates include that given by the uncertainties in  $T_{\text{eff}}$ ,  $\log g_*$  and  $\xi_t$ , as well as the scatter due to measurement and atomic data uncertainties.

The sky-projected stellar rotation velocity ( $v \sin I$ ) was determined by fitting the profiles of several unblended Fe I lines. We assumed a value for macroturbulence ( $v_{\text{mac}}$ ) of  $5.2 \pm 0.3 \text{ km s}^{-1}$ , based on the tabulation by Gray (2008), and we used an instrumental FWHM of  $0.06 \pm 0.01 \text{ \AA}$ , determined from the telluric lines around  $6300 \text{ \AA}$ . A best-fitting value of  $v \sin I = 7.6 \pm 0.4 \text{ km s}^{-1}$  was obtained. However, recent work by Bruntt et al. (2010) suggests a lower value for macroturbulence of  $v_{\text{mac}} = 4.2 \pm 0.3 \text{ km s}^{-1}$  which yields a slightly higher  $v \sin I = 8.1 \pm 0.4 \text{ km s}^{-1}$ . We therefore adopt the average of these two determinations,  $v \sin I = 7.9 \pm 0.6 \text{ km s}^{-1}$ , with the uncertainty being the quadrature addition of the individual uncertainties. If  $v_{\text{mac}} = 0 \text{ km s}^{-1}$ ,

**Table 2.** Stellar parameters from the spectroscopic analysis

Parameter	Value
$T_{\text{eff}}$	$6300 \pm 100 \text{ K}$
$\log g_*$	$4.4 \pm 0.1 \text{ (cgs)}$
$\xi_t$	$1.4 \pm 0.1 \text{ km s}^{-1}$
$v \sin I$	$7.9 \pm 0.6 \text{ km s}^{-1}$
[Fe/H]	$-0.20 \pm 0.09$
[Na/H]	$-0.24 \pm 0.04$
[Mg/H]	$-0.11 \pm 0.06$
[Si/H]	$-0.13 \pm 0.07$
[Ca/H]	$-0.03 \pm 0.08$
[Sc/H]	$-0.07 \pm 0.06$
[Ti/H]	$-0.10 \pm 0.09$
[V/H]	$-0.16 \pm 0.09$
[Cr/H]	$-0.20 \pm 0.08$
[Mn/H]	$-0.45 \pm 0.11$
[Ni/H]	$-0.25 \pm 0.08$
$\log A(\text{Li})[\text{LTE}]$	$2.82 \pm 0.08$
$\log A(\text{Li})[\text{NLTE}]$	$2.75 \pm 0.08$
$M_*$	$1.15 \pm 0.08 M_\odot$
$R_*$	$1.12 \pm 0.15 R_\odot$
R.A. (J2000)	$11^{\text{h}}17^{\text{m}}45.35^{\text{s}}$
Dec. (J2000)	$-19^\circ 03' 17.3''$
$V_{\text{mag}}$	$11.7 \pm 0.2$
$J_{\text{mag}}$	$10.91 \pm 0.02$
$H_{\text{mag}}$	$10.71 \pm 0.02$
$K_{\text{mag}}$	$10.65 \pm 0.03$
USNO-B1.0	0709-0239208
2MASS	11174536-1903171

**Note:** NLTE Lithium value using correction of Carlsson et al. (1994).  
Mass and Radius estimate using the Torres et al. (2010) calibration.

**Table 3.** Limb-darkening coefficients

Light curve (band)	$a_1$	$a_2$	$a_3$	$a_4$
WASP/Euler (RC)	0.430	0.488	-0.254	0.020
FTN (Pan-STARRS z)	0.520	0.060	0.100	-0.107

then a value of  $v \sin I = 8.7 \pm 0.4 \text{ km s}^{-1}$  is found, which is the upper-limit of the sky-projected rotation velocity.

#### 4. Combined analysis

The WASP, FTN and Euler photometry were combined with the CORALIE and HARPS radial velocities in a simultaneous Markov-chain Monte Carlo (MCMC) analysis (Collier Cameron et al. 2007; Pollacco et al. 2008). The transit light curve was modeled using the formulation of Mandel & Agol (2002) with the assumption that  $R_{\text{pl}} \ll R_*$ . Limb-darkening was accounted for using a four-coefficient nonlinear limb-darkening model, using fixed coefficients (Table 3) appropriate to the passbands and interpolated in effective temperature, surface gravity and metallicity from the tabulations of Claret (2000).

The transit light curve is parameterized by the epoch of midtransit  $T_0$ , the orbital period  $P$ , the planet-to-star area ratio  $(R_{\text{pl}}/R_*)^2$ , the approximate duration of the transit from initial to final contact  $T_{14}$ , and the impact parameter  $b = a \cos i/R_*$  (the distance, in fractional stellar radii, of the transit chord from the star's centre). The radial-velocity orbit is parameterized by the stellar reflex velocity semi-amplitude  $K_*$ , the systemic velocity  $\gamma$ , and  $\sqrt{e} \cos \omega$  and  $\sqrt{e} \sin \omega$  (Anderson et al. 2011a), where  $e$  is orbital eccentricity and  $\omega$  is the argument of periastron.

The linear scale of the system depends on the orbital separation  $a$  which, through Kepler's third law, depends on the stellar mass  $M_*$ . At each step in the Markov chain, the latest values of stellar density  $\rho_*$ , effective temperature  $T_{\text{eff}}$  and metallicity [Fe/H] are input in to the empirical mass calibration of Enoch et al. (2010) to obtain  $M_*$ . The shapes of the transit light curves (Seager & Mallén-Ornelas 2003) and the radial-velocity curve constrain  $\rho_*$ , which combines with  $M_*$  to give  $R_*$ .  $T_{\text{eff}}$  and [Fe/H] are proposal parameters constrained by Gaussian priors with mean values and variances derived directly from the stellar spectra (Table 2).

As the planet-star area ratio is constrained by the measured transit depth,  $R_{\text{pl}}$  follows from  $R_*$ . The planet mass  $M_{\text{pl}}$  is calculated from the measured value of  $K_1$  and  $M_*$ ; the planetary density  $\rho_{\text{pl}}$  and surface gravity  $\log g_{\text{pl}}$  then follow. We also calculate the blackbody equilibrium temperature  $T_{\text{eq}}$  (assuming zero albedo and efficient redistribution of heat from the planet's presumed permanent day side to its night side), the transit ingress and egress durations,  $T_{12}$  and  $T_{34}$ , and the orbital semi-major axis  $a$ .

At each step in the MCMC procedure, model transit light curves and radial-velocity curves are computed from the proposal parameter values, which are perturbed from the previous values by a small, random amount. The  $\chi^2$  statistic is used to judge the goodness of fit of these models to the data and a step is accepted if  $\chi^2$  is lower than for the previous step. A step with higher  $\chi^2$  is accepted with a probability  $\exp(-\Delta\chi^2/2)$ . In this way, the parameter space around the optimum solution is thoroughly explored. To give proper weighting to each transit and RV data set, the uncertainties are scaled at the start of the MCMC so as to obtain a reduced  $\chi^2$  of unity. We allow for a systematic instrumental offset,  $\Delta\gamma_{\text{HARPS}}$ , between the CORALIE and HARPS spectrographs.

From an initial MCMC fit for an eccentric orbit, we found  $e = 0.027^{+0.034}_{-0.020}$ , with a 3- $\sigma$  upper limit of 0.13. The  $F$ -test approach of Lucy & Sweeney (1971) indicates that there is a 66% probability that an eccentricity of or above the fitted value could have arisen by chance if the underlying orbit is in fact circular. As such, we impose a circular orbit, but we note that doing so has no significant effect as the fitted eccentricity was so small.

The median values and 1  $\sigma$  uncertainties of the system parameters derived from the MCMC model fit are presented in Table 4. The corresponding best-fitting transit light curves are shown in Figure 1 and Figure 3, and the best-fitting RV curve is shown in Figure 2.

Though the visual companion is 40 times fainter than WASP-31 and is resolved in the Euler and FTN images, we did correct the WASP photometry for the contamination prior to producing the MCMC solution presented. We checked the effect of the contamination by producing another MCMC solution using the non-corrected WASP photometry. The best-fitting parameter values were the same to within a tenth of an error bar.

Without exquisite photometry, our implementation of MCMC tends to bias the impact parameter, and thus  $R_*$  and  $R_{\text{pl}}$ , to higher values. This is because, with low-S/N photometry, the transit ingress and egress durations are uncertain, and symmetric uncertainties in those translate into asymmetric uncertainties in  $b$  and thus in  $R_*$ . The effect on the stellar and planetary radii is larger for high-impact-parameter planets such as WASP-31b. Therefore we explored an MCMC with a main-sequence (MS) prior imposed (Collier Cameron et al. 2007). This employs a Bayesian penalty to ensure that, in accepted steps, the values of stellar radius are consistent with the values of stellar mass for a main-sequence star. The differences between the solutions with

**Table 4.** System parameters from the combined analysis

Parameter (Unit)	Value
$P$ (d)	$3.4059096 \pm 0.000005$
$T_0$ (HJD)	$2455192.6887 \pm 0.0003$
$T_{14}$ (d)	$0.1103 \pm 0.0013$
$T_{12} = T_{34}$ (d)	$0.0285 \pm 0.0018$
$a/R_*$	$8.00 \pm 0.19$
$R_{\text{pl}}^2/R_*^2$	$0.01615 \pm 0.00027$
$b$	$0.780 \pm 0.013$
$i$ ( $^\circ$ )	$84.41 \pm 0.22$
$K_1$ ( $\text{m s}^{-1}$ )	$58.1 \pm 3.4$
$a$ (AU)	$0.04659 \pm 0.00035$
$e$	0 (adopted)
$\gamma_{\text{CORALIE}}$ ( $\text{m s}^{-1}$ )	$-124.923 \pm 0.035$
$\Delta\gamma_{\text{HARPS}}$ ( $\text{m s}^{-1}$ )	$-5.268 \pm 0.093$
$M_*$ ( $M_\odot$ )	$1.163 \pm 0.026$
$R_*$ ( $R_\odot$ )	$1.252 \pm 0.033$
$\rho_*$ ( $\rho_\odot$ )	$0.592 \pm 0.042$
$\log g_*$ (cgs)	$4.308 \pm 0.020$
$T_{\text{eff}}$ (K)	$6302 \pm 102$
[Fe/H]	$-0.200 \pm 0.090$
$M_{\text{pl}}$ ( $M_{\text{Jup}}$ )	$0.478 \pm 0.029$
$R_{\text{pl}}$ ( $R_{\text{Jup}}$ )	$1.549 \pm 0.050$
$\rho_{\text{pl}}$ ( $\rho_{\text{Jup}}$ )	$0.129 \pm 0.014$
$\log g_{\text{pl}}$ (cgs)	$2.659 \pm 0.036$
$T_{\text{eq1}}$ (K)	$1575 \pm 32$

and without MS priors are small and within errors, indicating that the transit light curves are of a quality such that the ingress and egress durations are measured sufficiently well. As such, we adopt the solution without the MS prior, which has slightly more conservative error bars.

## 5. System age

Using 2MASS photometry we constructed a colour-magnitude diagram (Figure 4) for WASP-31 and its common proper motion, K-type companion. A distance modulus of  $7.8 \pm 0.2$  ( $360 \pm 30$  pc) is required to place the companion on the main-sequence, which puts WASP-31 between the zero-age main sequence and 1-Gyr age lines. Thus, if the two stars are of common origin, they are most probably around 1-Gyr old, with an approximate upper age limit of 4 Gyr. Combining the absolute  $V_{\text{mag}}$  of an F7–8 star (Gray 2008) with the measured  $J - K$  and  $H - K$  colours of WASP-31 from 2MASS and the intrinsic colours from Koornneef (1983), we derive an interstellar extinction  $A_V = 0$  and a distance of  $360 \pm 20$  pc. This agreement with the distance determined from the colour-magnitude diagram supports the inference that the companion is associated with WASP-31 rather than being a mere line-of-sight neighbour. At a distance of 360 pc, the sky-projected separation of the two stars suggests that they would be separated by at least 12 600 AU (0.2 light-year).

Assuming aligned stellar-spin and planetary-orbit axes, the measured  $v \sin I$  of WASP-31 and its derived stellar radius indicate a rotational period of  $P_{\text{rot}} = 7.9 \pm 0.7$  d. Combining this with the  $B - V$  colour of an F8 star from Gray (2008), we used the relationship of Barnes (2007) to estimate a gyrochronological age of  $950 \pm 250$  Myr. This is an upper limit as the star would be rotating faster, and so be younger, than suggested by spectroscopic  $v \sin I$  if the stellar spin axis were inclined with respect to the sky plane. We used the method of Maxted et al. (2011)

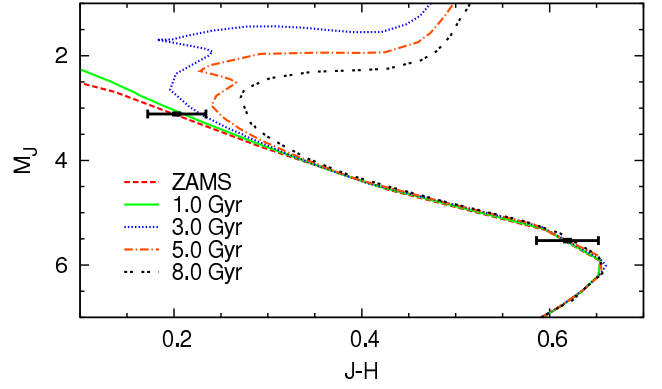


**Fig. 4.** Colour-magnitude diagram for WASP-31 and its companion. Various isochrones from Marigo et al. (2008) are given, with ages indicated in the figure. No de-reddening has been applied as  $A_V = 0$ .

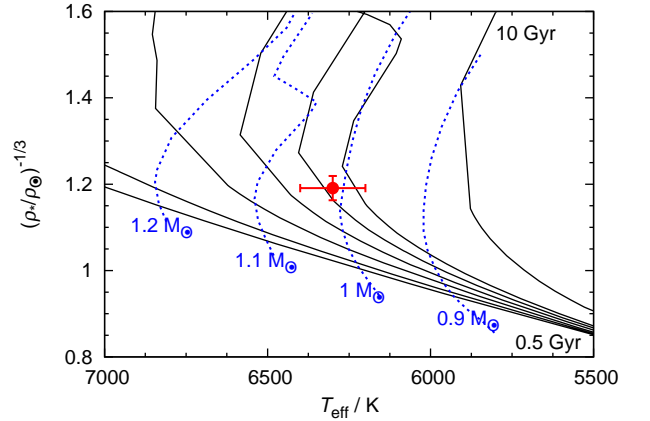


**Fig. 5.** Modified H-R diagram. The isochrones ( $Z = 0.012 \approx [\text{Fe}/\text{H}] = -0.20$ ) for the ages 0.5, 1, 2, 3, 4, 5 and 10 Gyr and the evolutionary mass tracks ( $Z = 0.012 \approx [\text{Fe}/\text{H}] = -0.20$ ;  $Y = 0.30$ ) are from Marigo et al. (2008). To obtain the mass tracks, we performed a simple linear interpolation of their  $Z = 0.0008$  and  $Z = 0.017$  tracks.

to search for rotational modulation of the WASP light curves, as can be caused by the combination of magnetic activity and stellar rotation. No evidence of modulation was found.

The lithium abundance ( $A_{\text{Li}} = 2.75 \pm 0.10$ ) found in WASP-31 implies an age (Sestito & Randich 2005) between that of open clusters such as M34 (250 Myr;  $A_{\text{Li}} = 2.92 \pm 0.13$ ) and NGC 752 (2 Gyr;  $A_{\text{Li}} = 2.65 \pm 0.13$ ). However, lithium is a poor indicator of age for a star as hot as WASP-31, and the measured abundance is consistent at the  $1-\sigma$  level with that of the upper envelope of the 5-Gyr M67 ( $A_{\text{Li}} = 2.55 \pm 0.18$ ).

We interpolated the stellar evolution tracks of Marigo et al. (2008) using  $\rho_*$  from the MCMC analysis and using  $T_{\text{eff}}$  and [Fe/H] from the spectral analysis (Figure 5). This suggests an age of  $4 \pm 1$  Gyr and a mass of  $1.0 \pm 0.1 M_\odot$  for WASP-31.

Taking account of each age indicator, we suggest a likely age of  $1_{-0.5}^{+3}$  Gyr.

## 6. Discussion

With a mass of  $0.48 M_{\text{Jup}}$  and a radius of  $1.55 R_{\text{Jup}}$ , WASP-31b has a density 13 per cent that of Jupiter and is  $\sim 0.3 R_{\text{Jup}}$

larger than predicted by standard models of irradiated gas giants (Fortney et al. 2007). Only WASP-17b (Anderson et al. 2010), which has a similar mass ( $0.49 M_{\text{Jup}}$ ), is known to have a lower density ( $0.06 \rho_{\text{Jup}}$ , Anderson et al. 2011b).

With an increasingly large sample of well-characterised planets, we can begin to make statistical inferences as to the physical reasons behind their diverse natures. Enoch et al. (2011) showed the radii of 16 of the 18 known low-mass ( $0.1\text{--}0.6 M_{\text{Jup}}$ ) planets strongly correlate with equilibrium temperature and host-star metallicity. The calibration of Enoch et al. (2011) predicts a radius of  $1.39 R_{\text{Jup}}$  for WASP-31b. In a similar study, but using a different metallicity dependence and treating the 74 known Jupiter-mass ( $0.2\text{--}2.5 M_{\text{Jup}}$ ) planets, Anderson & Iro (in prep.) also found a strong correlation between planetary radius and equilibrium temperature and host-star metallicity. The calibration of Anderson & Iro (in prep.) predicts a radius of  $1.23 R_{\text{Jup}}$  for WASP-31b. In each case, the predicted radius of WASP-31b is smaller than the measured radius ( $1.55 \pm 0.05 R_{\text{Jup}}$ ).

WASP-31 has a similarly low metallicity to WASP-17 ( $[\text{Fe}/\text{H}] = -0.19 \pm 0.09$ ; Triaud et al. 2010), thus both WASP-31b and WASP-17b could reasonably be expected to have small cores (Guillot et al. 2006; Burrows et al. 2007). However, this would only somewhat explain why the two planets are so large. Both planets are highly irradiated, with WASP-17b being more irradiated than WASP-31b as, despite being in a slightly wider orbit ( $a = 0.052 \text{ AU}$ ), its host star is larger ( $R_* = 1.58 R_{\odot}$ ) and hotter ( $T_{\text{eff}} = 6650 \text{ K}$ ; Anderson et al. 2011b). This results in an equilibrium temperature for WASP-17b hotter by 200 K than for WASP-31b and, from this, we could expect WASP-17b to be larger than WASP-31b. Both planets, though, are larger than predicted by standard models of irradiated giant planets (e.g. Fortney et al. 2007), and by the empirical relations of Enoch et al. (2011) and Anderson & Iro (in prep.). Hence, it seems likely that some additional physics, such as Ohmic heating (Batygin & Stevenson 2010), is at play.

The RV data place a stringent upper limit on WASP-31b's orbital eccentricity ( $e < 0.13$ ;  $3\sigma$ ). It is therefore unlikely that tidal heating resulting from the circularisation of an eccentric orbit (e.g. Bodenheimer et al. 2001) was responsible for significantly inflating the planet. However, we could happen to be viewing the system soon after circularisation occurred and prior to the planet significantly contracting. This would have made finding the planet easier due to the greater transit depth.

The metallicity of WASP-31 is at the lower end of what may be expected for a star of its age in the Solar neighbourhood (at a Galactocentric radius of 8.5 kpc; Magrini et al. 2009).

*Acknowledgements.* WASP-South is hosted by the South African Astronomical Observatory and we are grateful for their ongoing support and assistance. Funding for WASP comes from consortium universities and from the UK's Science and Technology Facilities Council. M. Gillon acknowledges support from the Belgian Science Policy Office in the form of a Return Grant.

## References

Anderson, D. R., Collier Cameron, A., Hellier, C., et al. 2011a, *ApJ*, 726, L19  
 Anderson, D. R., Hellier, C., Gillon, M., et al. 2010, *ApJ*, 709, 159  
 Anderson, D. R., Smith, A. M. S., Lanotte, A. A., et al. 2011b, *MNRAS*, 416, 2108  
 Baranne, A., Queloz, D., Mayor, M., et al. 1996, *A&AS*, 119, 373  
 Barnes, S. A. 2007, *ApJ*, 669, 1167  
 Batygin, K. & Stevenson, D. J. 2010, *ApJ*, 714, L238  
 Bodenheimer, P., Lin, D. N. C., & Mardling, R. A. 2001, *ApJ*, 548, 466  
 Bruntt, H., Bedding, T. R., Quirion, P., et al. 2010, *MNRAS*, 405, 1907  
 Burrows, A., Hubeny, I., Budaj, J., & Hubbard, W. B. 2007, *ApJ*, 661, 502  
 Carlsson, M., Rutten, R. J., Bruls, J. H. M. J., & Shchukina, N. G. 1994, *A&A*, 288, 860

Claret, A. 2000, *A&A*, 363, 1081  
 Collier Cameron, A., Pollacco, D., Street, R. A., et al. 2006, *MNRAS*, 373, 799  
 Collier Cameron, A., Wilson, D. M., West, R. G., et al. 2007, *MNRAS*, 380, 1230  
 Enoch, B., Cameron, A. C., Anderson, D. R., et al. 2011, *MNRAS*, 410, 1631  
 Enoch, B., Collier Cameron, A., Parley, N. R., & Hebb, L. 2010, *A&A*, 516, A33  
 Fortney, J. J., Baraffe, I., & Militzer, B. 2010, *Giant Planet Interior Structure and Thermal Evolution*, ed. S. Seager, 397–418  
 Fortney, J. J., Marley, M. S., & Barnes, J. W. 2007, *ApJ*, 659, 1661  
 Gillon, M., Smalley, B., Hebb, L., et al. 2009, *A&A*, 496, 259  
 Gray, D. F. 2008, *The Observation and Analysis of Stellar Photospheres*, ed. Gray, D. F. (Cambridge University Press)  
 Gu, P.-G., Lin, D. N. C., & Bodenheimer, P. H. 2003, *ApJ*, 588, 509  
 Guillot, T., Santos, N. C., Pont, F., et al. 2006, *A&A*, 453, L21  
 Guillot, T. & Showman, A. P. 2002, *A&A*, 385, 156  
 Hebb, L., Collier-Cameron, A., Loeillet, B., et al. 2009, *ApJ*, 693, 1920  
 Huéramo, N., Figueira, P., Bonfils, X., et al. 2008, *A&A*, 489, L9  
 Ibgui, L. & Burrows, A. 2009, *ApJ*, 700, 1921  
 Ibgui, L., Burrows, A., & Spiegel, D. S. 2010, *ApJ*, 713, 751  
 Ibgui, L., Spiegel, D. S., & Burrows, A. 2011, *ApJ*, 727, 75  
 Jackson, B., Greenberg, R., & Barnes, R. 2008, *ApJ*, 681, 1631  
 Koornneef, J. 1983, *A&A*, 128, 84  
 Leconte, J., Chabrier, G., Baraffe, I., & Levrard, B. 2010, *A&A*, 516, A64+  
 Li, J. & Goodman, J. 2010, *ApJ*, 725, 1146  
 Lucy, L. B. & Sweeney, M. A. 1971, *AJ*, 76, 544  
 Magain, P. 1984, *A&A*, 134, 189  
 Magrini, L., Sestito, P., Randich, S., & Galli, D. 2009, *A&A*, 494, 95  
 Mandel, K. & Agol, E. 2002, *ApJ*, 580, L171  
 Mandushev, G., O'Donovan, F. T., Charbonneau, D., et al. 2007, *ApJ*, 667, L195  
 Mardling, R. A. 2007, *MNRAS*, 382, 1768  
 Marigo, P., Girardi, L., Bressan, A., et al. 2008, *A&A*, 482, 883  
 Maxted, P. F. L., Anderson, D. R., Collier Cameron, A., et al. 2011, *PASP*, 123, 547  
 Pepe, F., Mayor, M., Queloz, D., et al. 2005, *The Messenger*, 120, 22  
 Perna, R., Menou, K., & Rauscher, E. 2010, *ApJ*, 719, 1421  
 Pollacco, D., Skillen, I., Collier Cameron, A., et al. 2008, *MNRAS*, 385, 1576  
 Pollacco, D. L., Skillen, I., Cameron, A. C., et al. 2006, *PASP*, 118, 1407  
 Queloz, D., Eggenberger, A., Mayor, M., et al. 2000a, *A&A*, 359, L13  
 Queloz, D., Henry, G. W., Sivan, J. P., et al. 2001, *A&A*, 379, 279  
 Queloz, D., Mayor, M., Weber, L., et al. 2000b, *A&A*, 354, 99  
 Roeser, S., Demleitner, M., & Schilbach, E. 2010, *AJ*, 139, 2440  
 Santos, N. C., Mayor, M., Naef, D., et al. 2002, *A&A*, 392, 215  
 Seager, S. & Mallén-Ornelas, G. 2003, *ApJ*, 585, 1038  
 Sestito, P. & Randich, S. 2005, *A&A*, 442, 615  
 Sozzetti, A., Torres, G., Charbonneau, D., et al. 2009, *ApJ*, 691, 1145  
 Torres, G., Andersen, J., & Giménez, A. 2010, *A&A Rev.*, 18, 67  
 Triaud, A. H. M. J., Collier Cameron, A., Queloz, D., et al. 2010, *A&A*, 524, A25+  
 Youdin, A. N. & Mitchell, J. L. 2010, *ApJ*, 721, 1113  
 Zacharias, N., Finch, C., Girard, T., et al. 2010, *AJ*, 139, 2184